Neural and behavioral control in *Caenorhabditis elegans* by a yellow-light–activatable caged compound

Hironori Takahashi[a,b], Mako Kamiya[a,c], Minoru Kawatani[a], Keitaro Umezawa[a], Yoshiaki Ukita[d], Shinsuke Niwa[e], Toshiyuki Oda[b,1], and Yasuteru Urano[a,f,g,1]

[a]Graduate School of Medicine, The University of Tokyo, Bunkyo-ku, 113-0033 Tokyo, Japan; [b]Department of Anatomy and Structural Biology, Graduate School of Medicine, University of Yamanashi, Chuo, 409-3898 Yamanashi, Japan; [c]Precursory Research for Embryonic Science and Technology (PRESTO), Japan Science and Technology Agency (JST), Kawaguchi, 332-0012 Saitama, Japan; [d]Department of Mechanical Engineering, University of Yamanashi, 400-8511 Kofu, Japan; [e]Frontier Research Institute for Interdisciplinary Sciences, Tohoku University, Aobaku, Sen-dai, 980-8578 Miyagi, Japan; [f]Graduate School of Pharmaceutical Sciences, The University of Tokyo, Bunkyo-ku, 113-0033 Tokyo, Japan; and [g]Core Research for Evolutional Science and Technology (CREST), Agency for Medical Research and Development (AMED), Chiyoda-ku, 100-0004 Tokyo, Japan

Edited by Iva Greenwald, Columbia University, New York, NY, and approved December 20, 2020 (received for review May 18, 2020)

Caenorhabditis elegans **is used as a model system to understand the neural basis of behavior, but application of caged compounds to manipulate and monitor the neural activity is hampered by the innate photophobic response of the nematode to short-wavelength light or by the low temporal resolution of photocontrol. Here, we develop boron dipyrromethene (BODIPY)-derived caged compounds that release bioactive phenol derivatives upon illumination in the yellow wavelength range. We show that activation of the transient receptor potential vanilloid 1 (TRPV1) cation channel by spatially targeted optical uncaging of the TRPV1 agonist *N*-vanillylnonanamide at 580 nm modulates neural activity. Further, neuronal activation by illumination-induced uncaging enables optical control of the behavior of freely moving *C. elegans* without inducing a photophobic response and without crosstalk between uncaging and simultaneous fluorescence monitoring of neural activity.**

caged compounds | *C. elegans* | photocontrol | fluorescence imaging | photolysis

Caged compounds that release bioactive molecules upon light irradiation have been widely used for photocontrol of cell signaling (1). Various molecules such as neurotransmitters, nucleotides, ions, drugs, fluorophores, and proteins can be rendered biologically inert by using photoreactive caging groups (2). Light irradiation induces photolysis of the caging groups to restore the bioactivity of these molecules. Since the initial applications of caged cyclic adenosine monophosphate (cAMP) (3) and caged adenosine triphosphate (ATP) (4) in biological experiments, caged compounds have been applied to cultured cells (1), brain slices (5, 6), and living animals (7). Although the light-mediated delivery of chemical probes in vivo is challenging, there are reports of photoactivation of neurons in *Drosophila* by caged ATP (8, 9) and photo-mediated gene activation in zebrafish by caged RNA/DNA (10, 11). The optical transparency of these species makes them particularly suitable targets for photochemical probes.

The nematode *Caenorhabditis elegans* is also amenable to optical manipulation using photocontrollable tools owing to its transparent body, compact nervous system, and ease of genetic manipulation (12–15). Nevertheless, few reports describe the application of caged compounds to *C. elegans*. One reason for this may be that most conventional caged compounds have the major limitation that uncaging requires short-wavelength (ultraviolet to blue) light, which induces an innate photophobic response, as well as causing cell damage or even death of the nematode (16, 17). Thus, it would be preferable to achieve photocontrol by using longer-wavelength visible light.

Methods for uncaging with longer-wavelength visible light (green to near infrared) include photorelease via metal–ligand photocleavage (18), via photooxidative C-C cleavage and hydrolysis (19), and by using a photosensitizer (20). However, these strategies have disadvantages: The photocages can only release the fluorophore upon irradiation at over 550 nm (18), the caged compounds show relatively poor temporal resolution of neural control due to the multistep nature of the photoreaction (19), and they generate toxic levels of reactive oxygen species under normoxic conditions (20). Therefore, they are unsuitable for neurophysiological experiments in *C. elegans*, a model system that is widely used to elucidate the neuronal basis of behavior. Another method for releasing bioactive molecules with visible/near-infrared light is to use two-photon excitation, wherein the excitation wavelength can be twice that of the one-photon counterpart (21–23). Two-photon excitation is particularly useful for studies that require spatially high-resolution uncaging, such as functional mapping of receptors along dendrites (6) and single-spine stimulation (24), although the amount of the photorelease is very small (25).

Here, we aimed to develop practically useful caged compounds that can be uncaged by one-photon excitation in *C. elegans* without the disadvantages described above and that would be suitable for neurophysiological experiments. We confirmed that our compounds exhibit sharp absorption spectra at around

Significance

Caged compounds that release bioactive molecules upon light irradiation are widely used by biologists. However, their application to neuroscientific research in the nematode *Caenorhabditis elegans* has been hampered by several drawbacks: Most of the caged compounds require short-wavelength light that induces an innate photophobic response, while red-shifted compounds show reduced temporal resolution of photocontrol or generate toxic levels of reactive oxygen species under normoxic conditions. We developed caged compounds based on a π-extended BODIPY derivative, Keio Fluors-1 (KFL-1), that releases an activator on yellow light illumination. This enables the behavior of *C. elegans* to be controlled by selectively activating specific neurons without inducing a photophobic response and without crosstalk between uncaging and fluorescence monitoring of neural activity.

Author contributions: H.T., M. Kamiya, T.O., and Y. Urano designed research; H.T., M. Kamiya, M. Kawatani, K.U., Y. Ukita, and S.N. performed research; H.T., Y. Ukita, and S.N. contributed new reagents/analytic tools; H.T., M. Kamiya, M. Kawatani, K.U., S.N., T.O., and Y. Urano analyzed data; and H.T., M. Kamiya, T.O., and Y. Urano wrote the paper.

The authors declare no competing interest.

This article is a PNAS Direct Submission.

[1]To whom correspondence may be addressed. Email: toda@yamanashi.ac.jp or uranokun@m.u-tokyo.ac.jp.

This article contains supporting information online at https://www.pnas.org/lookup/suppl/doi:10.1073/pnas.2009634118/-/DCSupplemental.

Published February 4, 2021.

580 nm that do not overlap with those of GFP-based probes and show simple, single-step photorelease of the caged molecules in response to light irradiation at over 550 nm. We also validated the application of caged *N*-vanillylnonanamide for neurophysiological studies. Uncaging by illumination at 580 nm with simultaneous monitoring of neuronal activity using GCaMP demonstrated that the uncaging triggers responses in sensory neurons, body wall muscles, motor neurons, and interneurons that are associated with behavioral changes of freely moving *C. elegans*.

Results

Initially, we focused on our previously developed 4-aryloxy boron dipyrromethene (BODIPY)–caged compounds, which can release phenols or bioactive molecules through cleavage of self-immolative linkers in response to irradiation with blue-green light (26, 27). Since uncaging with even longer-wavelength light can be accomplished by using π-extended BODIPY derivatives (26), we set out to develop caged compounds based on these derivatives. We focused on Keio Fluors-1 (KFL-1) as a caging group due to its red-shifted absorption (λ_{max}: 579 nm), sharp absorption spectrum, and high extinction coefficient (ε around 200,000 $M^{-1}\cdot cm^{-1}$) (28) compared to other BODIPY derivatives (26, 29).

We synthesized four KFL-1 derivatives (**1**–**4**) by incorporating aryl groups with different highest occupied molecular orbital (HOMO) energy levels at the boron position (Fig. 1 *A* and *B*). These KFL-1 derivatives showed strong and sharp absorption spectra with absorption maxima at 580 nm and molar extinction coefficients of 200,000 (*SI Appendix*, Fig. S1 and Table S1). We previously reported that the charge separation state formed by photoinduced electron transfer (PeT) from the aryl group to the fluorophore plays a critical role in the photocleavage of aryloxy BODIPY-caged compounds (26). The photoreaction of aryloxy KFL-1 derivatives is expected to proceed in the same manner, so we examined the PeT-based quenching of fluorescence (Fig. 1*C* and *SI Appendix*, Table S1). As expected, the fluorescence quantum efficiency (ϕ_{fl}) of aryloxy KFL-1 derivatives decreased as the HOMO energy level of the aryloxy groups increased. This means that the rate of PeT increases with increase in the HOMO energy level of the aryloxy group. However, a higher rate of PeT does not necessarily provide a high efficiency of uncaging, because back electron transfer may increase and compete with the uncaging reaction (26, 27). Indeed, we confirmed by high-performance liquid chromatography (HPLC) analysis that the

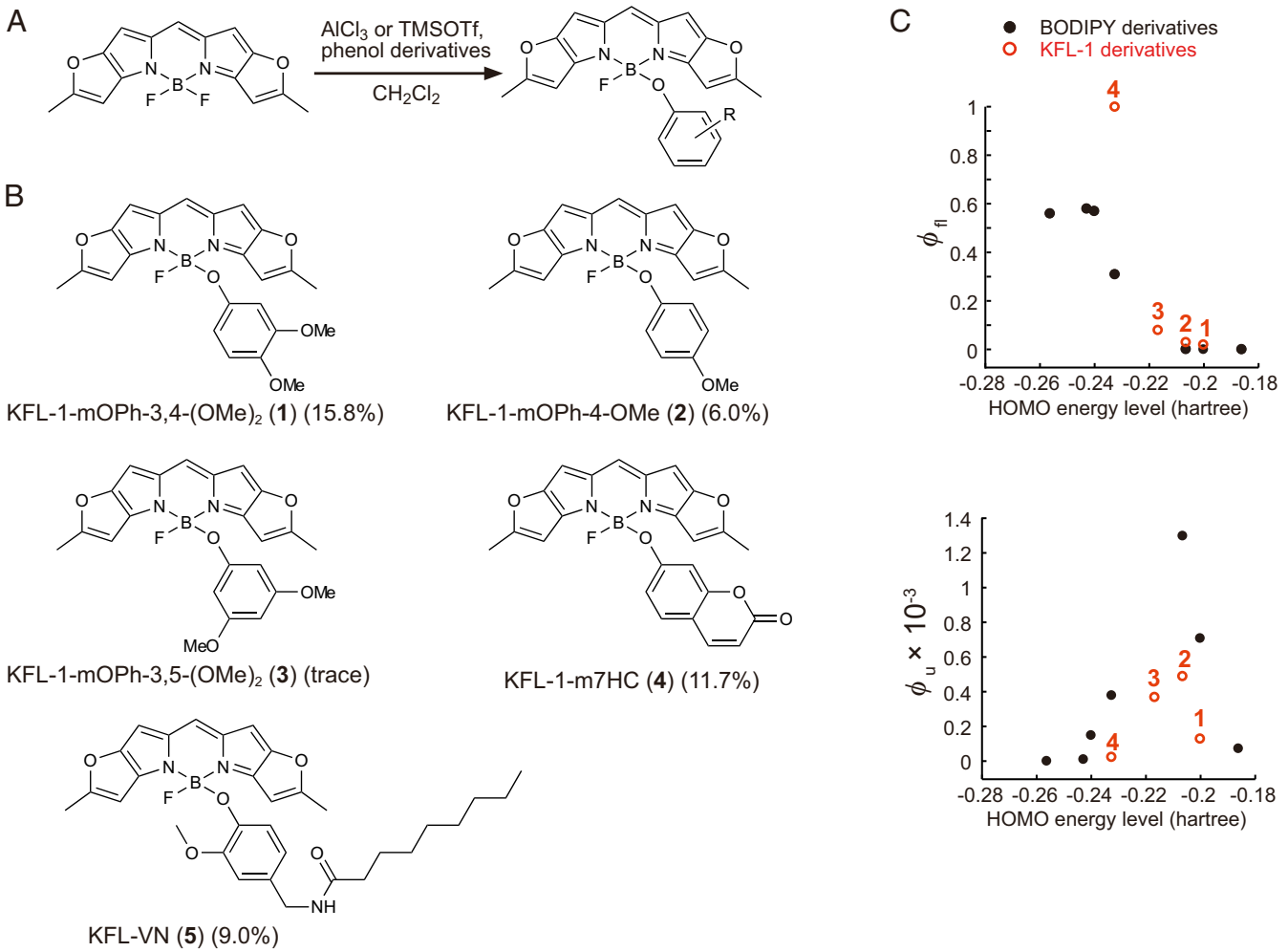

Fig. 1. Synthesis of aryloxy KFL-1 derivatives. (*A*) General scheme of the synthesis of aryloxy KFL-1 derivatives. (*B*) Aryloxy KFL-1 derivatives (**1**–**5**) synthesized in this study. (*C*) Plot of the fluorescence quantum efficiency (ϕ_{fl}) and uncaging quantum efficiency (ϕ_u) of aryloxy BODIPY or KFL-1 derivatives against the HOMO energy level of the corresponding phenols. The HOMO energy levels of the phenols were calculated (solvent = dichloromethane) at the B3LYP/6-31G level by Gaussian09. Black and red circles represent data of BODIPY-caged compounds (26) and KFL-1–caged compounds, respectively. The numerals on the red circles indicate aryloxy KFL-1 derivatives (**1**–**4**).

efficiency of photoclevage (ϕ_u) upon yellow light irradiation (580 ± 10 nm) increases with increasing HOMO energy level of the aryloxy groups up to −0.2 hartree and decreases above −0.2 hartree (Fig. 1*C* and *SI Appendix*, Figs. S2 and S3 and Table S1). Although the values of uncaging quantum efficiency (ϕ_u) of aryloxy KFL-1–caged compounds are lower than those of aryloxy BODIPY-caged compounds (0.00049 of KFL-1-mOPh-4-OMe vs. 0.0013 of BODIPY-OPhOMe) (26), the product of ε and ϕ_u, which represents the uncaging efficiency (2), is ∼100 $M^{-1}{\cdot}cm^{-1}$ due to compensation by the high molar absorption coefficient of the KFL-1 fluorophore (ε = 200,000; *SI Appendix*, Table S1) (28). This value of $\varepsilon\phi_u$ is of the same order of magnitude as that of the widely used *o*-nitrobenzyl caging group and other BODIPY-based caging groups (29).

As uncaging was most efficient when the HOMO energy level of the aryl group was around −0.21 hartree (Fig. 1*C*), we focused on a capsaicin analog, *N*-vanillylnonanamide (VN), whose HOMO energy level is −0.210 hartree [calculated with B3LYP/6-31G by Gaussian09 (solvent = dichloromethane)]. Capsaicin is an agonist of ligand-gated cation channel transient receptor potential vanilloid 1 (TRPV1) (30), and its caged derivative has been used to optically control the activity of nociceptive neurons in rats (31). Although wild-type *C. elegans* does not use capsaicin as a neurotransmitter and shows no acute response to capsaicin (32), VN binds to heterologously expressed TRPV1 and can induce selective activation in neurons of interest. Therefore, we next synthesized KFL-VN (**5**) by incorporating VN at the boron of KFL-1 (Fig. 1*B*) and examined its photochemical properties (Fig. 2*A*). KFL-VN showed a sharp absorption spectrum with a maximum around 577 nm, and the KFL-1–derived fluorescence was strongly suppressed (absorption maximum, λ_{abs} = 577 nm; emission maximum, λ_{em} = 587 nm; ϕ_{fl} = 0.01) (Fig. 2*B*). KFL-VN absorbs little light in the blue range (450–500 nm), so that excitation light for GCaMP should not induce photoactivation of KFL-VN (Fig. 2*B*). Liquid chromatography-mass spectrometry (LC/MS) analysis showed that KFL-VN was decomposed to produce VN and solvolysed KFL-1 upon irradiation with yellow light [time constant of consumption of KFL-VN, τ_c = 58 s; time constant of production of VN, τ_p = 78 s; ϕ_u = 0.00019 (calculated using τ_c); $\varepsilon\phi_u$ = 39 $M^{-1}{\cdot}cm^{-1}$ (ε was assumed to be 200,000 $M^{-1}{\cdot}cm^{-1}$, according to the literature (28).); chemical yield, 39.9 ± 4.8% (mean ± SEM, *n* = 3 independent measurements)] (Fig. 2 *A* and *C*). The chemical yield of VN was only up to 40%, probably owing to an unclarified photoinduced side reaction(s); however, the yield was sufficient to trigger neuronal responses. It should be noted that KFL-1–caged compounds are insoluble in aqueous solution. However, this problem can be overcome by solubilizing the compounds with ethanol/dodecane solution in the same way as described for long-chain lipids (33), as we previously reported (27). In *C. elegans*, the insolubility was overcome by delivering KFL-VN together with bacterial food as described below.

Next, we created worm strains expressing GCaMP6s in ASH sensory neurons under the *sra-6* promoter by microinjecting appropriate plasmids into wild-type or integrant worms expressing TRPV1 in ASH neurons (*kyIs200* X, kind gift from C. I. Bargmann, The Rockefeller University, New York) (32) to examine whether KFL-VN can induce neuronal activation in the worms in response to photoirradiation. Weak expression of GCaMP6s was also observed in ASI neurons (Fig. 3*A* and *SI Appendix*, *SI Note*). Next, KFL-VN was incorporated into worms by feeding a mixture of the compound and *Escherichia coli* (strain OP50), following the method used to deliver hydrophobic all-transretinal in optogenetic studies (14). By observing KFL-1–derived fluorescence with a confocal fluorescence microscope, we found that KFL-VN was localized mainly in the digestive system of the worm (buccal cavity, pharynx, and intestine) (Fig. 3*B*). Uncaging of KFL-VN was induced by yellow light irradiation (580 ± 20 nm) of the whole body of KFL-VN–fed *C. elegans*, and the fluorescence change of GCaMP6s was monitored during the photoirradiation. GCaMP6s fluorescence was increased in *kyIs200* X (TRPV1 (+), KFL-VN (+); onset latency, 1.62 ± 0.35 s), whereas no increase of fluorescence occurred in the absence of irradiation (Fig. 3 *C–E* and Movie S1). In averaged Ca^{2+} traces, wild-type worms with KFL-VN (TRPV1 (–), KFL-VN (+)) and *kyIs200* X with control compound **2** (TRPV1 (+), compound **2** (+)), which releases 4-methoxyphenol, showed modest increases in GCaMP fluorescence (∼20 and ∼25%, respectively) (Fig. 3*D*). However, the increases in these control groups were not statistically significant compared with the no irradiation group (Games–Howell method, *P* = 0.8115 (TRPV1 (–), KFL-VN (+) vs. TRPV1 (+), compound **2** (+)), 0.9074 (TRPV1 (–), KFL-VN (+) vs. no irradiation), and 0.9993 (TRPV1 (+), compound **2** (+) vs. no irradiation)) (Fig. 3*E*). Although the chemical yield of VN was not high (∼40%), these results indicated that no potentially interfering byproduct(s) was produced in the photoreaction, and thus we concluded that KFL-VN can be used for photocontrol of neural activity. Multiple light stimulations could also induce repetitive neuronal activation, although the magnitude of the

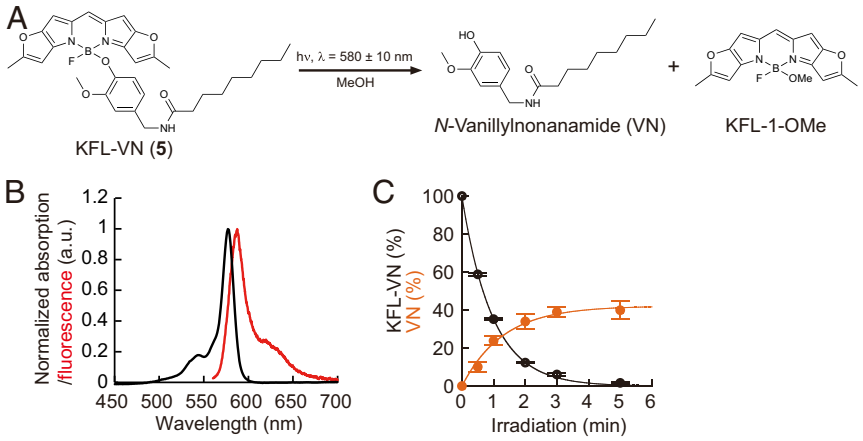

Fig. 2. Development of the KFL-1–caged TRPV1 agonist KFL-VN. (*A*) Scheme of uncaging reaction of KFL-VN. (*B*) Absorption (black line) and fluorescence (red line) spectra of KFL-VN. (*C*) Time course of KFL-VN consumption and VN production (580 ± 10 nm irradiation, 24.4 $mW{\cdot}cm^{-2}$). Data are presented as mean ± SEM from three independent measurements.

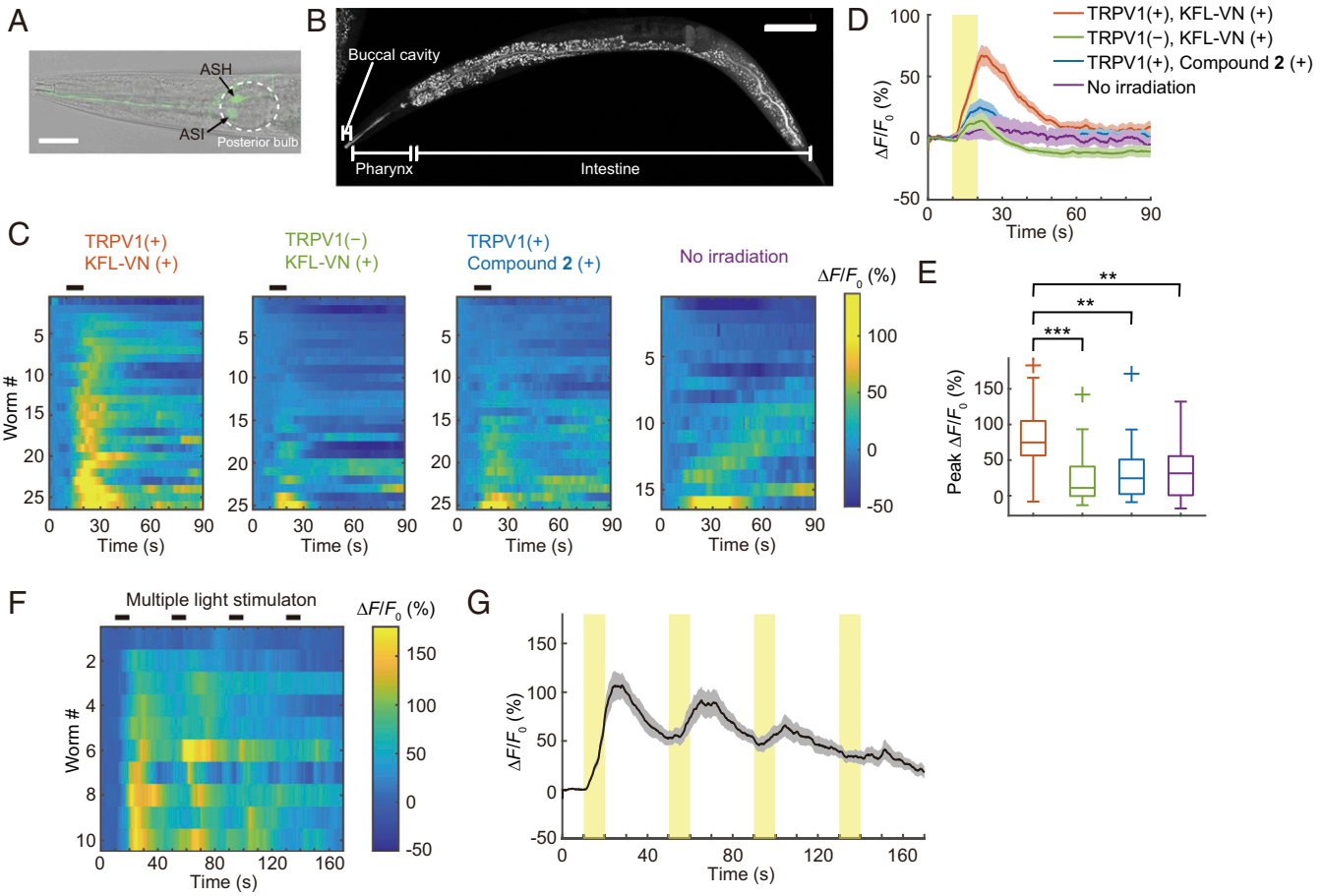

Fig. 3. Optical control of neuronal activity using KFL-VN. (*A*) ASH (strong fluorescence) and ASI (weak fluorescence) neurons expressing GCaMP6s in the worm head. (Scale bar, 25 μm.) (*B*) Maximum-intensity projection of a Z stack showing the distribution of KFL-VN in *C. elegans*. (Scale bar, 100 μm.) (*C*) Heat maps of ASH Ca^{2+} responses. Black bars above heat maps indicate light stimulation (10 s). Ca^{2+} responses are ordered by peak $\Delta F/F_0$. (*D*) Averaged Ca^{2+} responses from *C*. Light stimulation is indicated by a yellow bar. Shaded regions are SEM. (*E*) Box plots of peak Ca^{2+} responses: line inside the box, median; box edges, interquartile range; whiskers, range without outliers; cross mark, outliers. $^{**}P < 0.01$, $^{***}P < 0.001$, Games–Howell method ($P = 0.00009$ (TRPV1 (+), KFL-VN (+) vs. TRPV1 (–), KFL-VN (+)), 0.0016 (TRPV1 (+), KFL-VN (+) vs. TRPV1 (+), compound **2** (+)), 0.0037 (TRPV1 (+), KFL-VN (+) vs. no irradiation). $n = 26$ worms for TRPV1 (+), KFL-VN (+); 25 worms for TRPV1 (–), KFL-VN (+); 25 worms for TRPV1 (+), compound **2** (+); 16 worms for no irradiation. (*F*) Heat map of ASH Ca^{2+} responses to multiple light stimulations. Black bars above heat maps indicate light stimulation (10 s, 30 s interval, four times). Ca^{2+} responses are ordered by peak $\Delta F/F_0$. (*G*) Averaged Ca^{2+} responses from *F*. Light pulses are indicated by yellow bars. Shaded regions are SEM. $n = 10$ worms.

response decreased with repetition (Fig. 3 *F* and *G*). The reason for this may be desensitization of TRPV1, as reported in the case of repeated applications of capsaicin (30). In addition, although we focused on the cell body of neurons for quantifying neuronal activity, we also obtained calcium signals from the neurites in *kyIs200* X when the fluorescent images contained neurites on the same focal plane as the cell body (*SI Appendix*, Fig. S4). These results indicate that ASH neurons expressing TRPV1 were activated by VN released from yellow-light–activated KFL-VN, and this activation could be monitored in terms of the green fluorescence of GCaMP6s.

We tested whether the behavior of freely moving worms can be manipulated by optical uncaging of KFL-VN. After feeding KFL-VN to wild-type or *kyIs200* X strains, the whole body of the worms was repeatedly illuminated with 545–580 nm light, and their behavior was recorded and analyzed (Fig. 4*A*). Worms expressing TRPV1 exhibited an avoidance response with a reversal movement followed by an omega-shaped turn in response to light irradiation, but wild-type worms did not (Fig. 4 *B*–*E* and Movies S2 and S3). This irradiation-induced avoidance response is similar to the ASH-mediated acute response evoked by capsaicin application to *kyIs200* X (32). Repetitive light stimulation alone could elicit the avoidance response, but characteristically showed a decrease of the fraction responding to light and an increase in the response delay time with repetition (Fig. 4 *B* and *C*). These changes are due to sensory adaptation of ASH neurons to repetitive stimulation (34).

We also checked whether KFL-VN in the digestive system affects behavior, because enzymes in the intestine might cleave KFL-VN to release the agonist. Recording the behavior for 60 min using a microfluidic device established that KFL-VN does not induce the ASH-mediated reversal response in the absence of irradiation (*SI Appendix*, Fig. S5). The amount of KFL-VN in freely moving worms decreased with time, and after 60 min light irradiation could no longer effectively induce the reversal response (*SI Appendix*, Fig. S6).

Finally, we tested whether KFL-VN can be applied to other cells to optically manipulate their activity. We created worm strains expressing rat TRPV1 and GCaMP6s in body wall muscles (BWMs), motor neurons (HSN), interneurons (RIM, AVA), and sensory neurons (ASK). For BWM and HSN, optical manipulation was carried out with simultaneous recording of neuronal activity and behavior. In BWM with TRPV1 and KFL-VN, light irradiation induced Ca^{2+} influx into muscle cells and muscle

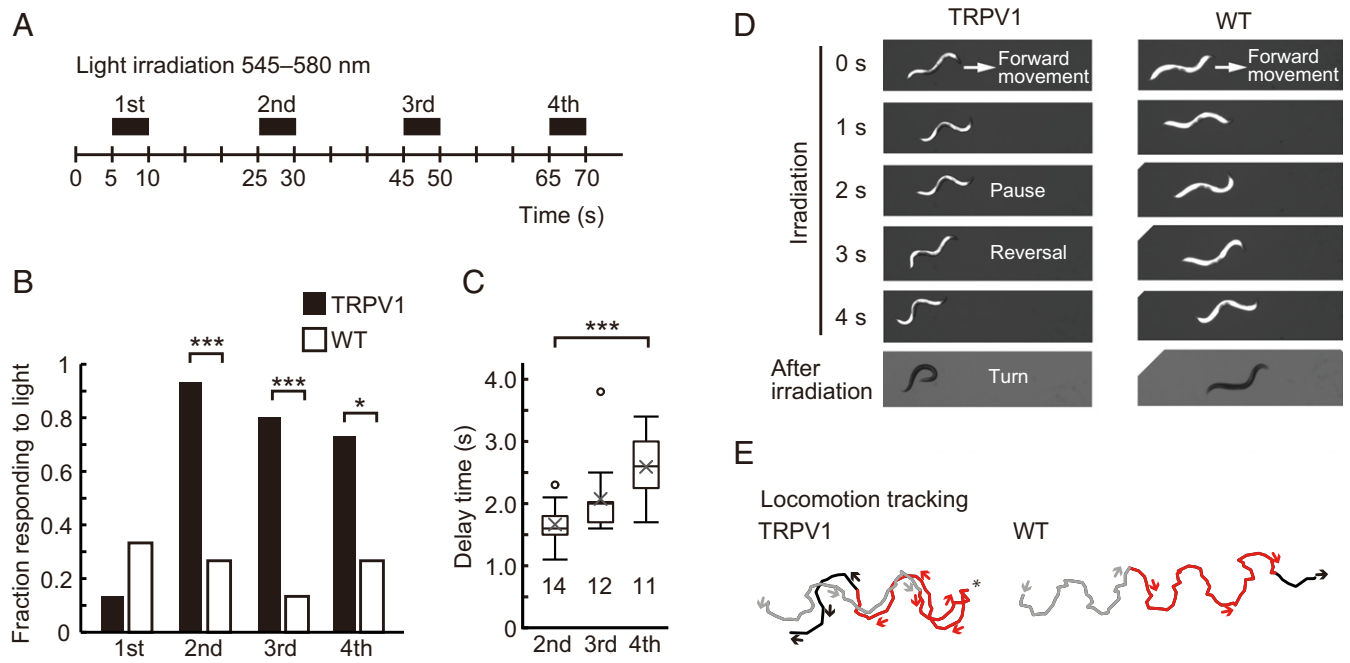

Fig. 4. Optical control of behavior by KFL-VN and whole-body illumination. (*A*) Timing schema for behavioral experiments. Before the experiments, worms were incubated on bacteria–KFL-VN (535 μM)–seeded nematode growth medium (NGM) plates for 30 min. After feeding, the worms were irradiated four times at 15-s intervals on unseeded NGM plates using a fluorescence stereomicroscope equipped with a mercury vapor lamp. (*B*) The fraction of *kyIs200* X (TRPV1) or wild-type (WT) worms showing backward movement during whole-body illumination was plotted (*kyIs200* X, 0.133 (first), 0.933 (second), 0.800 (third), 0.733 (fourth); WT, 0.333 (first), 0.267 (second), 0.133 (third), 0.267 (fourth)). Fifteen worms were examined for each strain. $*P < 0.05$, $***P < 0.001$, Fisher's exact test ($P = 0.3898$ (first), 0.0005 (second), 0.0007 (third), 0.0268 (fourth)). (*C*) Response delay time between the start of whole-body illumination and the initiation of backward movement. Data are shown as box plots: line inside the box, median; box edges, interquartile range; whiskers, range without outliers; open circles, outliers; cross mark, mean. The number under each plot indicates the number of worms examined. $***P < 0.001$, Games–Howell method ($P = 0.1079$ (second vs. third), 0.0007 (second vs. fourth), 0.1128 (third vs. fourth)). (*D*) Sequential images showing worm behavior during and after whole-body illumination. Upon uncaging of KFL-VN, TRPV1-expressing worms initiated backward movement, often followed by an omega turn, while wild-type worms continued forward movement. (*E*) Plots of the position of the head for tracking locomotion. Gray, red, and black lines denote before, during, and after whole-body illumination, respectively. Arrows and asterisks indicate the direction of movement and the starting point of reversal, respectively.

contraction, resulting in a transient decrease of relative body length (Fig. 5 *A–D* and Movie S4). In worms expressing TRPV1 in HSN neurons under the *egl-6* promoter, uncaging of KFL-VN strongly activated neuronal activity (HSN onset latency, 1.00 ± 0.16 s) and induced egg-laying behavior (Fig. 5 *E–J* and Movie S5), which is comparable to the results in the case of optogenetic manipulation of HSN neurons and egg laying (15, 35–38). Simultaneous imaging of Ca^{2+} and behavior showed that egg-laying events were synchronized with HSN activity (Fig. 5 *G* and *H*).

RIM or AVA interneurons play a crucial role in reversal initiation (14, 39). Thus, we tested whether RIM (Fig. 6*A*) or AVA (Fig. 6*E*) can be optically activated by KFL-VN and whether their activation can induce a reversal movement in freely moving worms expressing TRPV1 in these neurons. After feeding KFL-VN, Ca^{2+} imaging using GCaMP6s showed that uncaging of KFL-VN induced Ca^{2+} transients in RIM (RIM onset latency, 1.88 ± 0.75 s; Fig. 6 *B–D*) or AVA (AVA onset latency, 3.55 ± 0.77 s; Fig. 6 *F–H*). In freely moving worms, 65% of RIM::TRPV1 worms showed reversal responses to light. This result is comparable to that in a previous report of optogenetic RIM control on a wild-type background (14). In contrast, light illumination evoked reversal responses in only 35.3% of AVA::TRPV1 worms, which was not statistically significant compared to the control worms (Fig. 6*I*). This result may reflect the TRPV1 expression in multiple cells under the *rig-3* promoter (Fig. 6*E*) and their concomitant activation, as described previously (*SI Appendix*, *SI Note*) (40).

In addition to these cells, PVQ interneurons or glial cell GLRs also responded to uncaging of KFL-VN (*SI Appendix*, Fig. S7). We also applied KFL-VN to ASK sensory neurons, but we could not induce a sufficient Ca^{2+} response by light irradiation (*SI Appendix*, Fig. S8). This might be due to the weak expression of TRPV1 in ASK under the *sra-9* promoter, in contrast to the sufficient expression in HSN (*egl-6* promoter) (*SI Appendix*, Fig. S8*E*).

Discussion

Our results demonstrate that uncaging by yellow light enables optical control of neural activity and behavior in wild-type worms without inducing a photophobic response, and importantly, the absorption spectrum of KFL-VN is orthogonal to that of GCaMP, enabling imaging of GCaMP, even in neurites, to be done simultaneously without concomitant undesired photouncaging (*SI Appendix*, Figs. S4, S9*A*, and S10*D*). This caged compound activatable by light at a wavelength of 550 nm or longer has been applied to *C. elegans* for optical control of neural activity and behavior. In this context, KFL-1–caged compounds offer several advantages over other caged compounds that are activatable only by light over 550 nm. For example, caged compounds based on the cyanine scaffold show sustained release of the caged molecules even in the dark after photostimulation, due to the multistep nature of the reaction (19). This characteristic considerably reduces the temporal resolution of neural activation, and so these compounds are not well suited for photocontrol. In contrast, the KFL-1–caged compounds release phenol derivatives in a rapid, one-step photoreaction that occurs only during light irradiation (*SI Appendix*, Figs. S2 and S3). Silicon phthalocyanine (SiPc)–based compounds can also function

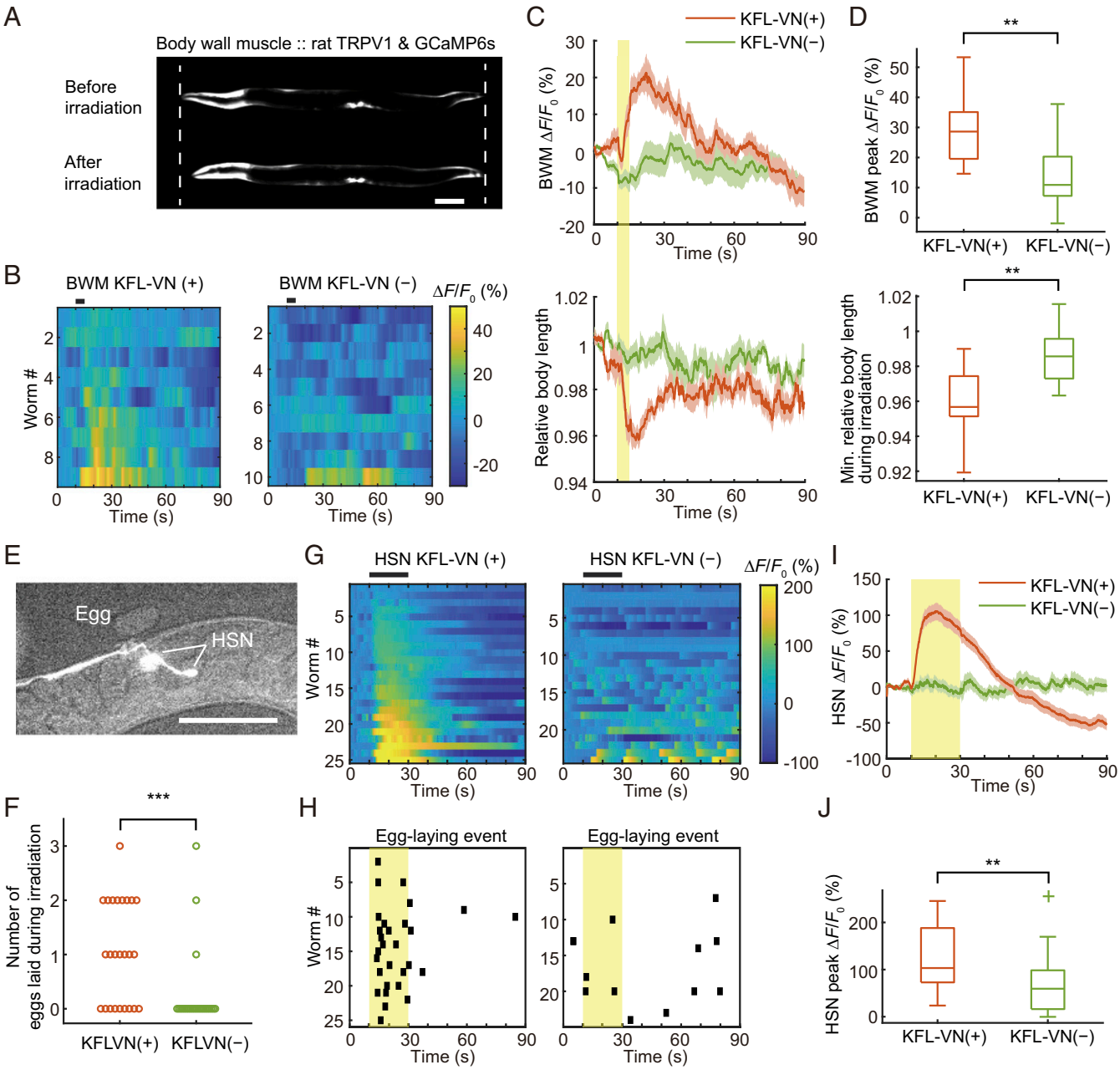

Fig. 5. Simultaneous imaging of neuronal activity and behavior with optical neuronal control. (*A*) Fluorescence image of GCaMP6s expressed in BWMs under the *myo-3* promoter. Dashed lines indicate the worm body length before irradiation. Scale bar, 100 μm. (*B*) Heat maps of BWM Ca^{2+} responses. Black bars above heat maps indicate light stimulation (5 s). Ca^{2+} responses are ordered by peak $\Delta F/F_0$. (*C*) Averaged Ca^{2+} responses from *B* and averaged relative body length. Light stimulation is indicated by a yellow bar. Shaded regions are SEM. (*D*) Box plots of peak Ca^{2+} responses and minimum relative body length during irradiation: line inside the box, median; box edges, interquartile range; whiskers, range without outliers. $^{**}P < 0.01$, Welch's *t* test ($P = 0.0084$ for peak $\Delta F/F_0$, 0.0082 for minimum relative body length). $n = 9$ worms for KFL-VN (+), 10 worms for KFL-VN (–). (*E*) Fluorescence image of GCaMP6s expressed in HSN neurons under the *egl-6* promoter. Scale bar, 100 μm. (*F*) Number of eggs laid during irradiation. $^{***}P < 0.001$, Mann–Whitney *U* test ($P = 0.0007$). (*G*) Heat maps of HSN Ca^{2+} responses. Black bars above heat maps indicate light stimulation (20 s). Ca^{2+} responses are ordered by peak $\Delta F/F_0$. (*H*) Plot of egg-laying event. Black points indicate the time that worms laid eggs. Light stimulation is indicated by yellow shaded regions. (*I*) Averaged Ca^{2+} responses from *G*. Light stimulation is indicated by a yellow bar. Shaded regions are SEM. (*J*) Box plots of peak Ca^{2+} responses: line inside the box, median; box edges, interquartile range; whiskers, range without outliers; cross mark, outliers. $^{**}P < 0.01$, Welch's *t* test ($P = 0.003$). $n = 25$ worms for KFL-VN (+), 24 worms for KFL-VN (–).

as caging groups under low-O_2 conditions and in the presence of an electron donor, but SiPcs essentially act as photosensitizers under normoxic conditions (20), whereas excitation of KFL-1–caged compounds did not cause any apparent cytotoxicity in worms under ambient conditions (Figs. 3–6).

Since *C. elegans* shows an innate photophobic response to intense short-wavelength light (16, 17), it is important to use longer-wavelength light for photocontrol. It is possible to use *lite-1* mutants lacking the light response (14, 41), but there is also a LITE-1–independent light response (16), and *lite-1* mutants show a slightly different locomotion pattern (42) and circadian rhythm (43) compared with normal nematodes. Our compounds can be activated by light at 580 nm and applied to *C. elegans* without inducing the photophobic response (16, 17).

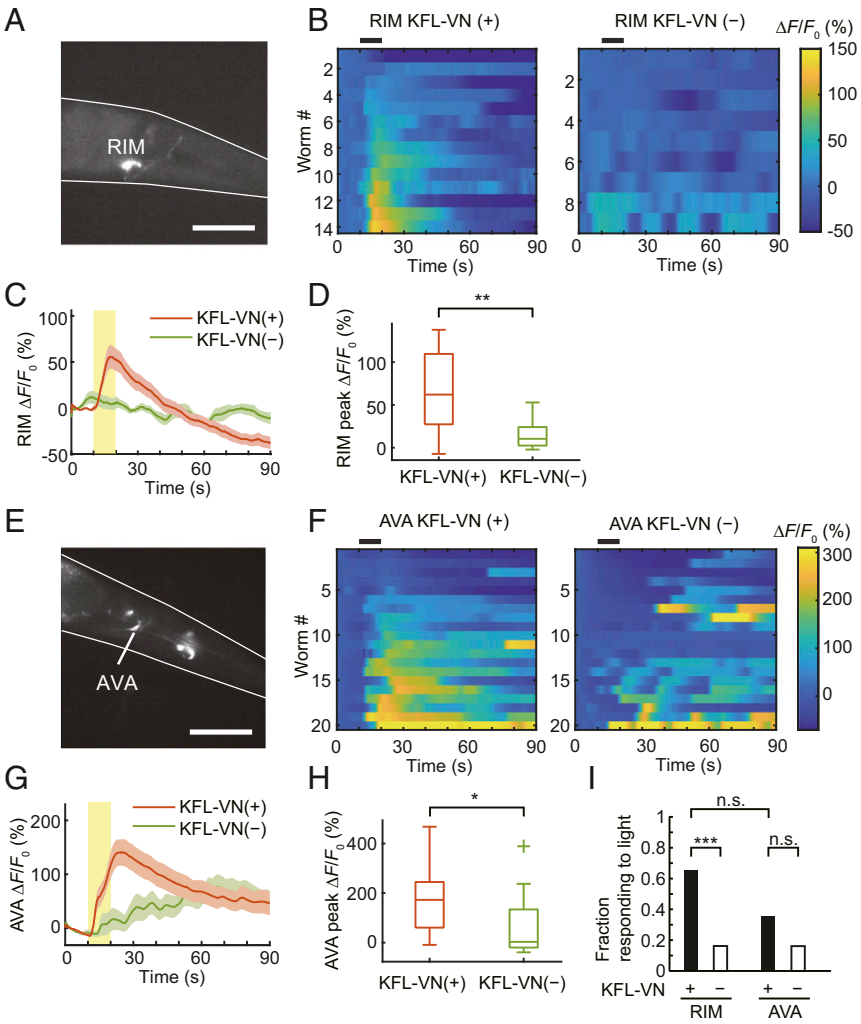

Fig. 6. Optical control of RIM and AVA interneurons. (*A*) Fluorescence image of GCaMP6s expressed in RIM neurons under the *tdc-1* promoter. Scale bar, 50 μm. (*B*) Heat maps of RIM Ca^{2+} responses. Black bars above heat maps indicate light stimulation (10 s). Ca^{2+} responses are ordered by peak $\Delta F/F_0$. (*C*) Averaged Ca^{2+} responses from *C*. Light stimulation is indicated by a yellow bar. Shaded regions are SEM. (*D*) Box plots of peak Ca^{2+} responses: line inside the box, median; box edges, interquartile range; whiskers, range without outliers. $^{**}P < 0.01$, Welch's *t* test ($P = 0.0022$). $n = 14$ worms for KFL-VN (+), 9 worms for KFL-VN (–). (*E*) Fluorescence image of GCaMP6s expressed in AVA neurons under *rig-3* promoter. Scale bar, 50 μm. (*F*) Heat maps of AVA Ca^{2+} responses. Black bars above heat maps indicate light stimulation (10 s). Ca^{2+} responses are ordered by peak $\Delta F/F_0$. (*G*) Averaged Ca^{2+} responses from *F*. Light stimulation is indicated by a yellow bar. Shaded regions are SEM. (*H*) Box plots of peak Ca^{2+} responses: line inside the box, median; box edges, interquartile range; whiskers, range without outliers; cross mark, outliers. $^{*}P < 0.05$, Welch's *t* test ($P = 0.0117$). $n = 20$ worms for KFL-VN (+), 20 worms for KFL-VN (–). (*I*) Plot of the fraction of RIM::TRPV1 or AVA::TRPV1 worms showing backward movement during whole-body illumination. $^{***}P < 0.001$, pairwise comparisons using Fisher's exact test ($P = 0.0001$ for RIM KFL-VN (+) vs. RIM KFL-VN (–), 0.2012 for AVA KFL-VN (+) vs. AVA KFL-VN (–), 0.0761 for RIM KFL-VN (+) vs. AVA KFL-VN (+)). $n = 40$ worms for RIM KFL-VN (+), 37 worms for RIM KFL-VN (–), 34 worms for AVA KFL-VN (+), 31 worms for AVA KFL-VN (–).

For photocontrol of neural signaling, optogenetics with genetically encoded, light-gated ion channels (channelrhodopsins [ChRs]) (44–46) offers an alternative to caged compounds. Since the first application to *C. elegans* (12), this approach has been widely used in neurophysiological research (14, 41, 47–49). Although simultaneous optical control and monitoring of neural activity in independent color channels have been hampered by spectral overlaps between ChRs and genetically encoded calcium indicators (GECIs) (14), recently developed red-shifted GECIs (50) have enabled simultaneous control and monitoring of neural activity with blue-activatable ChRs (*SI Appendix*, Fig. S10*A*) (41). However, red GECIs show smaller maximal fluorescence changes (three- to fourfold less) than green GECIs such as GCaMP6 indicators (50). In *C. elegans* interneurons, most of the synaptic connections are located on the neurites (51) and the confinement of neuronal activity to the neurites is important for sensory and motor processing (41, 52–56). Since neuronal microcompartments such as neurites show a weaker fluorescence signal (57), it is advantageous to use high-performance green GECIs such as GCaMP6 and jGCaMP7 indicators that show large maximal fluorescence changes (10- to 14-fold) (58, 59) to detect the compartmentalized Ca^{2+} transients with a sufficient signal-to-noise ratio. However, red-shifted optogenetic actuators such as VChR1 (60), C1V1 (61), Chrimson (62), and ReaChR (63) have a long tail on the blue side of their excitation spectra, resulting in undesired activation at the wavelengths used to excite green GECIs (*SI Appendix*, Figs. S9*A* and S10 *B* and *C*), as described previously (48). Our compounds enable simultaneous imaging of green GECIs in neurites without crosstalk (*SI Appendix*, Figs. S4, S9*A*, and S10*D*) and thus can serve in a complementary role with optogenetics.

The combination of caged compounds and optogenetics is very efficient, as described previously (64). For example, the KFL-1 caging group can be used for direct protection of neuromodulators such as serotonin and dopamine that have a phenolic structure or for indirect protection of amino acids and amines such as glutamate, γ (gamma)-aminobutyric acid (GABA), and histamine through a benzyloxycarbonyl linker (26). Thus, KFL-1 caged neuromodulators working at 580 nm and blue-light sensitive ChRs working at 480 nm can be combined without optical crosstalk for analyses of neural functions. In addition, the sharp absorption spectra of KFL-1 and BODIPY caged compounds should enable multicolor photolysis and calcium imaging, in which neuronal activity would be excited by KFL-VN at 580 nm, or inhibited by BODIPY-histamine (26) and histamine-gated chloride channel (HisCl) (65) at 500 nm, and simultaneously monitored using XCaMP-B (66) at 400 nm (*SI Appendix*, Fig. S9*B*).

Materials and Methods

Detailed materials and methods are provided in *SI Appendix, SI Methods*. This includes information on chemical synthesis, spectroscopic measurements, quantification of photoreaction, worm strains, molecular biology, calcium imaging, image processing, behavioral assays, data analysis, and microfluidic device fabrication. Aryloxy KFL-1 derivatives were synthesized as previously reported (26, 27). For experiments using *C. elegans*, standard culture, molecular biology, and microinjection techniques were used.

Data Availability. All study data are included in this article and/or supporting information.

ACKNOWLEDGMENTS. This research was supported in part by Japan Agency for Medical Research and Development (AMED) under Grant Number JP19gm0710008 (to Y. Urano), by Japan Science and Technology Agency (JST) / Precursory Research for Embryonic Science and Technology (PRESTO) Grant JPMJPR14F8 (to M. Kamiya); by Ministry of Education, Culture, Sports, Science and Technology (MEXT) / Japan Society for the Promotion of Science (JSPS) KAKENHI Grants JP16H02606, JP26111012, and JP19H05632 (to Y. Urano), JP17H05057 (to T.O.), and JP16H06536 (to S.N.); by the JSPS Core-to-Core Program, A. Advanced Research Networks (JPJSCCA20170007, to Y. Urano), JP15H05951 and JP20H05724 (to M. Kamiya) and JP15J05894 and JP19K16291 (to H.T.); by the Takeda Science Foundation (T.O.); by the Naito Foundation (T.O.); by the Uehara Memorial Foundation (T.O.); by the Senri Life Science Foundation (T.O.); by Daiichi Sankyo Foundation of Life Science (to T.O.); by The Association for Fordays Self-Reliance Support in Japan (grant to H.T.); and by The Konica Minolta Science and Technology Foundation (grant to H.T.). We are grateful to T. Yazaki at the Center for Creative Technology, University of Yamanashi, for expert technical assistance. We thank K. Ohmae, R. Kousaka, N. Takahashi, N. Maruyama, T. Kubo, M. Bam, N. Kanou, M. Kirikae, and members of the Y. Urano and T.O. laboratories for their technical help and valuable discussions.

1. G. C. R. Ellis-Davies, Caged compounds: Photorelease technology for control of cellular chemistry and physiology. *Nat. Methods* **4**, 619–628 (2007).
2. C. Brieke, F. Rohrbach, A. Gottschalk, G. Mayer, A. Heckel, Light-controlled tools. *Angew. Chem. Int. Ed. Engl.* **51**, 8446–8476 (2012).
3. J. Engels, E. J. Schlaeger, Synthesis, structure, and reactivity of adenosine cyclic 3′,5′-phosphate benzyl triesters. *J. Med. Chem.* **20**, 907–911 (1977).
4. J. H. Kaplan, B. Forbush 3rd, J. F. Hoffman, Rapid photolytic release of adenosine 5′-triphosphate from a protected analogue: Utilization by the Na:K pump of human red blood cell ghosts. *Biochemistry* **17**, 1929–1935 (1978).
5. G. C. Ellis-Davies, M. Matsuzaki, M. Paukert, H. Kasai, D. E. Bergles, 4-Carboxymethoxy-5,7-dinitroindolinyl-Glu: An improved caged glutamate for expeditious ultraviolet and two-photon photolysis in brain slices. *J. Neurosci.* **27**, 6601–6604 (2007).
6. M. Matsuzaki, T. Hayama, H. Kasai, G. C. R. Ellis-Davies, Two-photon uncaging of gamma-aminobutyric acid in intact brain tissue. *Nat. Chem. Biol.* **6**, 255–257 (2010).
7. R. Durand-de Cuttoli *et al*., Optofluidic control of rodent learning using cloaked caged glutamate. *Proc. Natl. Acad. Sci. U.S.A.* **117**, 6831–6835 (2020).
8. J. D. Clyne, G. Miesenböck, Sex-specific control and tuning of the pattern generator for courtship song in *Drosophila*. *Cell* **133**, 354–363 (2008).
9. S. Q. Lima, G. Miesenböck, Remote control of behavior through genetically targeted photostimulation of neurons. *Cell* **121**, 141–152 (2005).
10. H. Ando, T. Furuta, R. Y. Tsien, H. Okamoto, Photo-mediated gene activation using caged RNA/DNA in zebrafish embryos. *Nat. Genet.* **28**, 317–325 (2001).
11. H. Ando *et al*., Lhx2 mediates the activity of Six3 in zebrafish forebrain growth. *Dev. Biol.* **287**, 456–468 (2005).
12. G. Nagel *et al*., Light activation of channelrhodopsin-2 in excitable cells of *Caenorhabditis elegans* triggers rapid behavioral responses. *Curr. Biol.* **15**, 2279–2284 (2005).
13. J. F. Liewald *et al*., Optogenetic analysis of synaptic function. *Nat. Methods* **5**, 895–902 (2008).
14. Z. V. Guo, A. C. Hart, S. Ramanathan, Optical interrogation of neural circuits in *Caenorhabditis elegans*. *Nat. Methods* **6**, 891–896 (2009).
15. A. M. Leifer, C. Fang-Yen, M. Gershow, M. J. Alkema, A. D. T. Samuel, Optogenetic manipulation of neural activity in freely moving *Caenorhabditis elegans*. *Nat. Methods* **8**, 147–152 (2011).
16. S. L. Edwards *et al*., A novel molecular solution for ultraviolet light detection in *Caenorhabditis elegans*. *PLoS Biol.* **6**, e198 (2008).
17. A. Ward, J. Liu, Z. Feng, X. Z. Xu, Light-sensitive neurons and channels mediate phototaxis in *C. elegans*. *Nat. Neurosci.* **11**, 916–922 (2008).
18. T. A. Shell, J. R. Shell, Z. L. Rodgers, D. S. Lawrence, Tunable visible and near-IR photoactivation of light-responsive compounds by using fluorophores as light-capturing antennas. *Angew. Chem. Int. Ed. Engl.* **53**, 875–878 (2014).
19. A. P. Gorka, R. R. Nani, J. Zhu, S. Mackem, M. J. Schnermann, A near-IR uncaging strategy based on cyanine photochemistry. *J. Am. Chem. Soc.* **136**, 14153–14159 (2014).
20. E. D. Anderson, A. P. Gorka, M. J. Schnermann, Near-infrared uncaging or photosensitizing dictated by oxygen tension. *Nat. Commun.* **7**, 13378 (2016).
21. B. Guillaume, G. Thibault, O. David, From one-photon to two-photon probes: "Caged" compounds, actuators, and photoswitches. *Angew. Chem. Int. Ed.* **52**, 4526–4537 (2013).
22. C. Tran *et al*., Two-photon "caging" groups: Effect of position isomery on the photorelease properties of aminoquinoline-derived photolabile protecting groups. *Org. Lett.* **17**, 402–405 (2015).
23. E. B. Brown, J. B. Shear, S. R. Adams, R. Y. Tsien, W. W. Webb, Photolysis of caged calcium in femtoliter volumes using two-photon excitation. *Biophys. J.* **76**, 489–499 (1999).
24. M. Matsuzaki, N. Honkura, G. C. Ellis-Davies, H. Kasai, Structural basis of long-term potentiation in single dendritic spines. *Nature* **429**, 761–766 (2004).
25. J. M. Amatrudo, J. P. Olson, H. K. Agarwal, G. C. R. Ellis-Davies, Caged compounds for multichromic optical interrogation of neural systems. *Eur. J. Neurosci.* **41**, 5–16 (2015).
26. N. Umeda *et al*., Boron dipyrromethene as a fluorescent caging group for single-photon uncaging with long-wavelength visible light. *ACS Chem. Biol.* **9**, 2242–2246 (2014).
27. M. Kawatani, M. Kamiya, H. Takahashi, Y. Urano, Factors affecting the uncaging efficiency of 500 nm light-activatable BODIPY caging group. *Bioorg. Med. Chem. Lett.* **28**, 1–5 (2018).
28. K. Umezawa, Y. Nakamura, H. Makino, D. Citterio, K. Suzuki, Bright, color-tunable fluorescent dyes in the visible-near-infrared region. *J. Am. Chem. Soc.* **130**, 1550–1551 (2008).
29. J. A. Peterson *et al*., Family of BODIPY photocages cleaved by single photons of visible/near-infrared light. *J. Am. Chem. Soc.* **140**, 7343–7346 (2018).
30. M. J. Caterina *et al*., The capsaicin receptor: A heat-activated ion channel in the pain pathway. *Nature* **389**, 816–824 (1997).
31. D. Gilbert *et al*., Caged capsaicins: New tools for the examination of TRPV1 channels in somatosensory neurons. *ChemBioChem* **8**, 89–97 (2007).
32. D. M. Tobin *et al*., Combinatorial expression of TRPV channel proteins defines their sensory functions and subcellular localization in *C. elegans* neurons. *Neuron* **35**, 307–318 (2002).
33. C. E. Chalfant *et al*., Long chain ceramides activate protein phosphatase-1 and protein phosphatase-2A. Activation is stereospecific and regulated by phosphatidic acid. *J. Biol. Chem.* **274**, 20313–20317 (1999).
34. M. A. Hilliard *et al*., *In vivo* imaging of *C. elegans* ASH neurons: Cellular response and adaptation to chemical repellents. *EMBO J.* **24**, 63–72 (2005).
35. K. M. Collins *et al*., Activity of the *C. elegans* egg-laying behavior circuit is controlled by competing activation and feedback inhibition. *eLife* **5**, e21126 (2016).
36. L. Emtage *et al*., IRK-1 potassium channels mediate peptidergic inhibition of *Caenorhabditis elegans* serotonin neurons via a $G(_o)$ signaling pathway. *J. Neurosci.* **32**, 16285–16295 (2012).
37. B. Ravi, J. Garcia, K. M. Collins, Homeostatic feedback modulates the development of two-state patterned activity in a model serotonin motor circuit in *Caenorhabditis elegans*. *J. Neurosci.* **38**, 6283–6298 (2018).
38. J. C. Brewer, A. C. Olson, K. M. Collins, M. R. Koelle, Serotonin and neuropeptides are both released by the HSN command neuron to initiate *Caenorhabditis elegans* egg laying. *PLoS Genet.* **15**, e1007896 (2019).
39. A. Gordus, N. Pokala, S. Levy, S. W. Flavell, C. I. Bargmann, Feedback from network states generates variability in a probabilistic olfactory circuit. *Cell* **161**, 215–227 (2015).
40. C. Schmitt *et al*., Specific expression of channelrhodopsin-2 in single neurons of *Caenorhabditis elegans*. *PLoS One* **7**, e43164 (2012).
41. W. Steuer Costa *et al*., A GABAergic and peptidergic sleep neuron as a locomotion stop neuron with compartmentalized Ca2+ dynamics. *Nat. Commun.* **10**, 4095 (2019).
42. S. J. Husson, A. Gottschalk, A. M. Leifer, Optogenetic manipulation of neural activity in *C. elegans*: From synapse to circuits and behaviour. *Biol. Cell* **105**, 235–250 (2013).
43. M. E. Goya, A. Romanowski, C. S. Caldart, C. Y. Bénard, D. A. Golombek, Circadian rhythms identified in *Caenorhabditis elegans* by in vivo long-term monitoring of a bioluminescent reporter. *Proc. Natl. Acad. Sci. U.S.A.* **113**, E7837–E7845 (2016).
44. E. S. Boyden, F. Zhang, E. Bamberg, G. Nagel, K. Deisseroth, Millisecond-timescale, genetically targeted optical control of neural activity. *Nat. Neurosci.* **8**, 1263–1268 (2005).

45. G. Nagel *et al*., Channelrhodopsin-1: A light-gated proton channel in green algae. *Science* **296**, 2395–2398 (2002).
46. G. Nagel *et al*., Channelrhodopsin-2, a directly light-gated cation-selective membrane channel. *Proc. Natl. Acad. Sci. U.S.A.* **100**, 13940–13945 (2003).
47. M. Guo *et al*., Reciprocal inhibition between sensory ASH and ASI neurons modulates nociception and avoidance in *Caenorhabditis elegans*. *Nat. Commun.* **6**, 5655 (2015).
48. J. Larsch *et al*., A circuit for gradient climbing in *C. elegans* chemotaxis. *Cell Rep.* **12**, 1748–1760 (2015).
49. F. B. Shipley, C. M. Clark, M. J. Alkema, A. M. Leifer, Simultaneous optogenetic manipulation and calcium imaging in freely moving *C. elegans*. *Front. Neural Circuits* **8**, 28 (2014).
50. H. Dana *et al*., Sensitive red protein calcium indicators for imaging neural activity. *eLife* **5**, e12727 (2016).
51. J. G. White, E. Southgate, J. N. Thomson, S. Brenner, The structure of the nervous system of the nematode *Caenorhabditis elegans*. *Philos. Trans. R. Soc. Lond. B Biol. Sci.* **314**, 1–340 (1986).
52. D. A. Clark, D. Biron, P. Sengupta, A. D. T. Samuel, The AFD sensory neurons encode multiple functions underlying thermotactic behavior in *Caenorhabditis elegans*. *J. Neurosci.* **26**, 7444–7451 (2006).
53. S. H. Chalasani *et al*., Dissecting a circuit for olfactory behaviour in *Caenorhabditis elegans*. *Nature* **450**, 63–70 (2007).
54. S. H. Chalasani *et al*., Neuropeptide feedback modifies odor-evoked dynamics in *Caenorhabditis elegans* olfactory neurons. *Nat. Neurosci.* **13**, 615–621 (2010).
55. S. Oda, M. Tomioka, Y. Iino, Neuronal plasticity regulated by the insulin-like signaling pathway underlies salt chemotaxis learning in *Caenorhabditis elegans*. *J. Neurophysiol.* **106**, 301–308 (2011).
56. M. Hendricks, H. Ha, N. Maffey, Y. Zhang, Compartmentalized calcium dynamics in a *C. elegans* interneuron encode head movement. *Nature* **487**, 99–103 (2012).
57. J. Larsch, D. Ventimiglia, C. I. Bargmann, D. R. Albrecht, High-throughput imaging of neuronal activity in *Caenorhabditis elegans*. *Proc. Natl. Acad. Sci. U.S.A.* **110**, E4266–E4273 (2013).
58. T. W. Chen *et al*., Ultrasensitive fluorescent proteins for imaging neuronal activity. *Nature* **499**, 295–300 (2013).
59. H. Dana *et al*., High-performance calcium sensors for imaging activity in neuronal populations and microcompartments. *Nat. Methods* **16**, 649–657 (2019).
60. F. Zhang *et al*., Red-shifted optogenetic excitation: A tool for fast neural control derived from *Volvox carteri*. *Nat. Neurosci.* **11**, 631–633 (2008).
61. O. Yizhar *et al*., Neocortical excitation/inhibition balance in information processing and social dysfunction. *Nature* **477**, 171–178 (2011).
62. N. C. Klapoetke *et al*., Independent optical excitation of distinct neural populations. *Nat. Methods* **11**, 338–346 (2014).
63. J. Y. Lin, P. M. Knutsen, A. Muller, D. Kleinfeld, R. Y. Tsien, ReaChR: A red-shifted variant of channelrhodopsin enables deep transcranial optogenetic excitation. *Nat. Neurosci.* **16**, 1499–1508 (2013).
64. J. P. Olson, M. R. Banghart, B. L. Sabatini, G. C. Ellis-Davies, Spectral evolution of a photochemical protecting group for orthogonal two-color uncaging with visible light. *J. Am. Chem. Soc.* **135**, 15948–15954 (2013).
65. N. Pokala, Q. Liu, A. Gordus, C. I. Bargmann, Inducible and titratable silencing of *Caenorhabditis elegans* neurons in vivo with histamine-gated chloride channels. *Proc. Natl. Acad. Sci. U.S.A.* **111**, 2770–2775 (2014).
66. M. Inoue *et al*., Rational engineering of XCaMPs, a multicolor GECI suite for in vivo imaging of complex brain circuit dynamics. *Cell* **177**, 1346–1360.e24 (2019).